Acta Crystallographica Section B
Structural Science
ISSN 0108-7681

Phase transitions in $K_2Cr_2O_7$ and structural redeterminations of phase II

T. J. R. Weakley,[a] E. R. Ylvisaker,[b] R. J. Yager,[b] J. E. Stephens,[b] R. D. Wiegel,[b] M. Mengis,[c] M. R. Bauer,[b] P. Wu,[b] P. Photinos[b] and S. C. Abrahams[b]*

[a]Department of Chemistry, University of Oregon, Eugene, OR 97403, USA, [b]Physics Department, Southern Oregon University, Ashland, OR 97520, USA, and [c]North Medford High School, Medford, OR 97504, USA

Correspondence e-mail: sca@mind.net

Received 14 July 2004
Accepted 20 September 2004

Crystals of phase II $K_2Cr_2O_7$, potassium dichromate, space group $P\overline{1}$, grown from aqueous solution undergo a first-order transition to phase I, space group reportedly $P2_1/n$, at a phase-transition temperature, T_{PT}, of 544 (2) K on first heating; the corresponding transition on cooling is at 502 (2) K. The endotherm on subsequent heatings occurs reproducibly at T_{PT} = 531 (2) K. Mass loss between *ca* 531 and 544 K, identified as included water, is rapid and continues more slowly to higher temperatures for a total loss of *ca* 0.20%. The higher T_{PT} on first heating is associated with the increasing pressure of superheated water occupying inclusion defects. The latent diagonal glide plane in phase II allows the structure of phase I to be inferred. The triclinic structure at 296 K has been independently redetermined. Normal probability analysis shows high consistency between the resulting and previous atomic coordinates, but with uncertainties reduced by a factor of *ca* 2. The earlier uncertainties are systematically underestimated by a comparable factor. The structure of phase II*b*, space group *A*2/*a* on transposing axes, was determined at *ca* 300 K by Krivovichev *et al.* [*Acta Cryst.* (2000), C**56**, 629–630]. The first-order transition between phases I and II arises from the *ca* 60° relative rotation of terminal O atoms in each tetrahedron as the *n* glide plane is gained or lost. A transition between phases II*b* and I, also of first order, is likely but not between phases II and II*b*. An intermediate phase may exist between phases II*b* and I.

1. Introduction

The prediction that $K_2HCr_2AsO_{10}$ is a new ferroelectric with $T_c \simeq 560$ K (Abrahams, 2003), based on the atomic coordinates determined by Averbuch-Pouchot *et al.* (1978), led to its preparation, calorimetry and dielectric measurement. The initial growth of $K_2HCr_2AsO_{10}$ crystals from the reaction between $K_2Cr_2O_7$ and $As_2O_5{\cdot}xH_2O$ with $x \simeq 3$ was usually followed by the subsequent formation of triclinic phase II (see *Appendix A* for the IUCr phase nomenclature) of $K_2Cr_2O_7$, the preparation of which was first reported by Mitscherlich (1830). Groth (1908) showed that phase II could be grown either from aqueous solution or from the melt; he determined the morphology and noted that crystals grown from the melt crumble to a powder at 513 K. Shubnikov (1912, 1931) reported a difference in growth on the (001) and (00$\overline{1}$) faces of triclinic phase II crystals, for which a mechanism has been presented by Silber *et al.* (1999).

Numerous subsequent investigations into the properties of polymorphic $K_2Cr_2O_7$ have been summarized by Klement & Schwab (1960), who also measured the lattice constants of monoclinic phase (I) at 573 K and determined its space group as $P2_1/n$, see Table 1.

Table 1
Unit-cell dimensions in $K_2Cr_2O_7$ phase I, transposed phase II*b* and phase II.

Transposed phase II*b*: from $abc_{\text{Krivovichev } et\ al.\ (2000)}$ to $cb\bar{c}$ in a transposed cell.

Phase	*a* (Å)	*b* (Å)	*c* (Å)	α (°)	β (°)	γ (°)	Space group
I	7.55†	7.52	13.45	90	91.68	90	$P2_1/n$
II*b*	7.4672 (10)	7.3750 (10)	13.0339 (17)	90	88.077 (2)	90	$A2/a$
II	7.3837 (8)	7.4622 (6)	13.3949 (12)	96.204 (7)	98.046 (8)	90.943 (8)	$P\bar{1}$

† At 573 K; dimensional uncertainties not given by Klement & Schwab (1960).

Kuz'min *et al.* (1967, 1969) first reported the structure determination of triclinic phase (II), lopezite, in space group $P\bar{1}$, followed by Brandon & Brown (1968) and later by Brunton (1973). The Raman and IR spectra of phase II were measured by Mathur *et al.* (1968) and the space group confirmed by Carter & Bricker (1969). Jaffray & Labary (1956) observed an endotherm in 'pure' II-$K_2Cr_2O_7$ at T_{PT} = 542 (2) K and an exotherm at 513 K; after melting, the endotherm was noted at 528 (2) K, the exotherm remaining unchanged at 513 K on cooling. The phase-transition entropy change in $K_2Cr_2O_7$ at 528 (2) K was given by Klement & Schwab (1960) as *ca* 5 J mol^{-1} K^{-1}. Hess & Eysel (1989) reported the phase transition at T_{PT} = 526 K to be of first order, with the entropy change ΔS = 2.85 J mol^{-1} K^{-1}. They labelled the monoclinic phase I as α, the triclinic phase II as β and gave the change in unit-cell volume $\Delta V_{I-II} = \{[V(\text{phase I}) - V(\text{phase II})]/V(\text{phase I, phase II})_{av}\} \simeq 0.015$ at T_{PT}.

Zhukova & Pinsker (1964) used electron diffraction to determine the space group of the monoclinic phase (II*b*) formed at *ca* 300 K by slow crystallization from dilute aqueous solution on a collodion support. The unit-cell dimensions reported do not differ significantly from those in Table 1,[1] but the actual space group was not recognized. Krivovichev *et al.* (2000) prepared phase II*b* at temperatures close to ambient, labelled it β and determined its structure; Krivovichev & Burns (2003) also grew this phase from a reaction between K_2CrO_4 and $(UO_2)(NO_3)_2(H_2O)_6$. A transition at *ca* 325 K from the monoclinic phase (*i.e.* II*b*) was proposed by Kozlova *et al.* (1978) on the basis of an IR study. A detailed morphological study of triclinic $K_2Cr_2O_7$, presented by Stedehouder & Terpstra (1930), noted the reversed order of the *a* and *b* axes in phases II and II*b*.

Transitions between phases I and II, I and II*b*, and II and II*b* are investigated structurally in the present report together with a calorimetric and thermogravimetric study of the transition between phases II and I. The term II*b* designates a phase with some stability in a thermal range overlapping that of phase II and a transition path to phase I that differs from the path between phases II and I. Recent reports of a new 'chiral' phase (Suda & Matsushita, 2004) are consistent with the model presented for this system. The structure of stable phase II has been redetermined in duplicate as a contribution to the study of statistical descriptors and analysis in crystallography, *cf.* Schwarzenbach *et al.* (1989). The results are compared quantitatively with those of earlier determinations and are used in the phase transition investigations.

2. Experimental

2.1. Sample preparation and crystal growth

Stoichiometric quantities of crystalline $K_2Cr_2O_7$ and $As_2O_5{\cdot}xH_2O$, with 99.9% purity and $x \simeq 3$ from Sigma–Aldrich, were dissolved in H_2O (2:1:100 mol), in a variant of the method of Averbuch-Pouchot *et al.* (1978) in preparing $K_2HCr_2AsO_{10}$, see §1. The resulting solution was heated to boiling for several minutes, then allowed to cool to room temperature. Two crops of strongly reddish-orange[2] crystals commonly formed. The first exhibited hexagonal morphology, with X-ray powder patterns corresponding to $K_2HCr_2AsO_{10}$, the second formed rather equidimensional crystals of low symmetry over a period of *ca* 6 days. Several crystals from two second-growth batches were examined diffractometrically and identified by X-ray powder diffraction as II-$K_2Cr_2O_7$. All had unit-cell dimensions with $a \simeq 7.38$, $b \simeq 7.46$, $c \simeq 13.40$ Å, $\alpha \simeq 96.2$, $\beta \simeq 98.1$ and $\gamma \simeq 90.9°$ in space group $P\bar{1}$. A crystal from each second growth batch was selected for study, see Table 2.

Phase II*b*-$K_2Cr_2O_7$ was prepared (Krivovichev *et al.*, 2000; Kir'yanova, 2004) by cooling saturated aqueous solutions of K_2CrO_4 and $K_2Cr_2O_7$ at 300.8 K, with K_2O:CrO_3:H_2O = 19.17:20.67:60.16 wt %, to 283–288 K at a rate of 3–6 K min^{-1}; the crystals formed are reported as stable in excess of 1 year at room temperature.

2.2. Solubility

The solubility of II-$K_2Cr_2O_7$ at 298 K is 128 (3) g l^{-1}. Values in the literature include 49 g l^{-1} at 273 K and 1020 g l^{-1} at 373 K (Weast *et al.*, 1988). An exponential fit gives the result in Fig. 1. The initial formation of $K_2HCr_2AsO_{10}$ crystals with a solubility at 298 K of 205 (5) g l^{-1}, followed by the later growth of less soluble $K_2Cr_2O_7$ crystals, is attributed to the depletion of the $K_2Cr_2O_7$ concentration by the reaction with $As_2O_5{\cdot}xH_2O$.

2.3. Diffraction data

Diffraction data from two crystals of $K_2Cr_2O_7$ phase II were collected at 296(2) K with a Nonius CAD-4 serial diffract-

[1] For a unit cell with a = 7.47 (1), b = 7.35 (2), c = 12.94 (2) Å and β = 91.92 (17)°.

[2] ISCC-NBS Color (Supplement to NBS Circular 553). The complete list of terms with RGB values is given at http://swiss.csail.mit.edu/~jaffer/Color/nbs-iscc-rgb.txt and also http://tx4.us/nbs-iscc.htm.

Table 2
Experimental details.

	Crystal 1	Crystal 2
Crystal data		
Chemical formula	$K_2Cr_2O_7$	$K_2Cr_2O_7$
M_r	294.18	294.18
Cell setting, space group	Triclinic, $P\bar{1}$	Triclinic, $P\bar{1}$
a, b, c (Å)	7.3807 (9), 7.4593 (11), 13.3910 (16)	7.3837 (8), 7.4622 (6), 13.3949 (12)
α, β, γ (°)	96.205 (11), 98.033 (10), 90.914 (12)	96.204 (7), 98.046 (8), 90.943 (8)
V (Å^3)	725.37 (16)	726.12 (12)
Z	4	4
D_x (Mg m^{-3})	2.694	2.691
Radiation type	Mo $K\alpha$	Mo $K\alpha$
No. of reflections for cell parameters	25	25
θ range (°)	14.0–15.0	14.0–14.7
μ (mm^{-1})	4.13	4.13
Temperature (K)	296	296
Crystal form, color	Block, strongly reddish-orange	Block, strongly reddish-orange
Crystal size (mm)	0.27 × 0.20 × 0.14	0.25 × 0.20 × 0.15
Data collection		
Diffractometer	Nonius CAD-4 serial	Nonius CAD-4 serial
Data collection method	ω–2θ	ω–2θ
Absorption correction	Part of the refinement model (ΔF)	Part of the refinement model (ΔF)
T_{min}	0.382	0.386
T_{max}	0.560	0.538
No. of measured, independent and observed reflections	4533, 4227, 4096	2759, 2544, 2253
Criterion for observed reflections	$I > 1.00\sigma(I)$	$I > 1.00\sigma(I)$
R_{int}	0.011	0.020
θ_{max} (°)	30.0	25.0
Range of h, k, l	$0 \Rightarrow h \Rightarrow 10$ $-10 \Rightarrow k \Rightarrow 10$ $-18 \Rightarrow l \Rightarrow 18$	$0 \Rightarrow h \Rightarrow 8$ $-8 \Rightarrow k \Rightarrow 8$ $-15 \Rightarrow l \Rightarrow 15$
No. and frequency of standard reflections	3 every 300 reflections	3 every 300 reflections
Refinement		
Refinement on	F^2	F^2
$R[F^2 > 2\sigma(F^2)]$, $wR(F^2)$, S	0.025, 0.040, 1.74	0.029, 0.042, 1.95
No. of reflections	4227	2544
No. of parameters	200	200
H-atom treatment	No H atoms present	No H atoms present
Weighting scheme	$w = 4F_o^2/[\sigma^2(I) + (0.025I)^2]$	$w = 4F_o^2/[\sigma^2(I) + (0.020I)^2]$
$(\Delta/\sigma)_{max}$	0.020	0.008
$\Delta\rho_{max}$, $\Delta\rho_{min}$ (e Å^{-3})	0.49, −0.40	0.61, −0.45
Extinction method	Zachariasen (1967)	Zachariasen (1967)
Extinction coefficient	1.27×10^{-6}	3.6×10^{-7}

Computer programs used: *CAD*-4/*PC* (Enraf–Nonius, 1993), *TeXsan* (Molecular Structure Corporation, 1997).

ometer in the ω–2θ mode. The intensities of three control reflections showed no significant variation. Other experimental details are given in Table 2.

2.4. Structural redetermination of II-$K_2Cr_2O_7$

The structure was solved by the use of a *SIR*92 E-map (Altomare *et al.*, 1994). Empirical absorption corrections were applied using *DIFABS* (Walker & Stuart, 1983), based on the structure as refined with isotropic displacement parameters. Corrections based on azimuthal scans did not lead to a significant reduction in residuals or standard uncertainties (s.u.s) and analytical corrections were precluded by the irregular crystal form. We have found the results of corrections made with *DIFABS* for $\mu < 5$ mm^{-1} are comparable with those made analytically, a conclusion supported by the minor residual systematic error in atomic coordinates detected in §4.[3] The structure solution from each data set was independent of any in the literature; each was confirmed by the examination of the Patterson function. Refined site-occupancy factors did not differ significantly from unity for either crystal. The final value of a Zachariasen-type (1967) secondary extinction parameter was $1.27\ (12) \times 10^{-6}$ for crystal 1, $3.6\ (2) \times 10^{-7}$ for crystal 2, see also Table 2 and §3.1. All calculations used the *TeXsan* program suite (Molecular Structure Corporation, 1997).

3. Structure of phases II-$K_2Cr_2O_7$, II*b*-$K_2Cr_2O_7$ and I-$K_2Cr_2O_7$

3.1. Phase II

The structure of II-$K_2Cr_2O_7$, the most common stable phase at room temperature, contains four independent CrO_4 tetrahedra per unit cell, pairs of which share common O4 or O11 atoms resulting in two sets of independent $Cr_2O_7^{2-}$ ions, see Figs. 2 and 3 (Dowty, 2003), and also the coordinates in Table S1.[4] The averaged $d_{Cr-Oshared}$ = 1.784 (7) Å is significantly much longer than the three terminal d_{Cr-O} in each tetrahedron, *i.e.* $\langle d_{Cr-O}\rangle_{terminal}$ = 1.612 (7) Å. The bridging angles are ∠ Cr1—O4—Cr2 = 127.1 (3) and ∠ Cr3—O11—Cr4 = 124.1 (2)°. The four independent K atoms are coordinated by 7–10 nearest O atoms. Selected interatomic distances are presented in Table 3.

3.2. Phase II*b*

The unit cell of II*b*-$K_2Cr_2O_7$ (Krivovichev *et al.*, 2000) contains a single independent CrO_4 tetrahedron, pairs of

[3] See discussion in http://www.chem.gla.ac.uk/~louis/software/wingx/absorb.html.
[4] Supplementary data for this paper are available from the IUCr electronic archives (Reference: BK0147). Services for accessing these data are described at the back of the journal.

which share a common O3 atom on the twofold axis to form $Cr_2O_7^{2-}$ ions with the bridging angle ∠ Cr—O3—Cr = 123.3 (1)°, see Figs. 4 and 5, and also Table S1 of the supplementary material. The K atom has nine nearest O atoms within the limit $d_{K-O} \leq 3.5$ Å. The transposed unit-cell dimensions in space group *A*2/*a* are given in Table 1.

3.3. Phase I

The unit-cell dimensions of monoclinic phase I at 573 K are comparable to those of phases II and II*b*, see Table 1. The structure of phase I has not yet been determined experimentally, but may be reconstructed from the latent glide plane discernible in phase II, see Figs. 2 and 3, and also Table S1, assuming pairs of atoms related by the *n* glide plane in phase I undergo equal but opposite displacements at the transition. Phase I is derived from phase II rather than phase II*b* to eliminate bias caused by the possible existence of an intermediate phase between II*b* and I, see §6.3. The pairs of atoms that are pseudosymmetrically related in phase II are K1 and K3, K2 and K4, Cr1 and Cr4, Cr2 and Cr3, and also O1–O7 and O12, O14, O13, O11, O8, O10, O9, respectively. All O atoms are labelled in Fig. S1 of the supplementary material. The coordinates of a given atom in phase I are taken as the average of those resulting from the application of the *n* glide plane to one member of an atomic pair and the original coordinates of the other member, see Table 4. The loss of the *n* glide plane on cooling through T_{PT} is accompanied by a relative rotation of *ca* 60° about the O_{shared}—Cr— axis by the terminal O atoms; the onset barrier to rotation is probably related to the first-order phase transition, see §6.2. The resulting structure is presented in Figs. 6 and 7, with an uncertainty in atomic positions estimated as *ca* 0.1 Å.

Orientational differences between averaged tetrahedra in phase II cause dimensional distortions in the inferred positions of the tetrahedra in phase I, with $\langle d_{Cr-O} \rangle$ = 1.47 Å in $Cr1O_4$, 1.48 Å in $Cr2O_4$, for the three terminal bonds and d_{Cr-O}(shared) = 1.61, 1.58 Å. All *d* values based on Table 4 have an uncertainty of *ca* 0.17 Å and are 0.15 Å less than those determined in phases II and I*b*, with the intertetrahedral angle ∠ Cr1—O4—Cr2 = 138° about 12° larger, *cf.* §3.4.

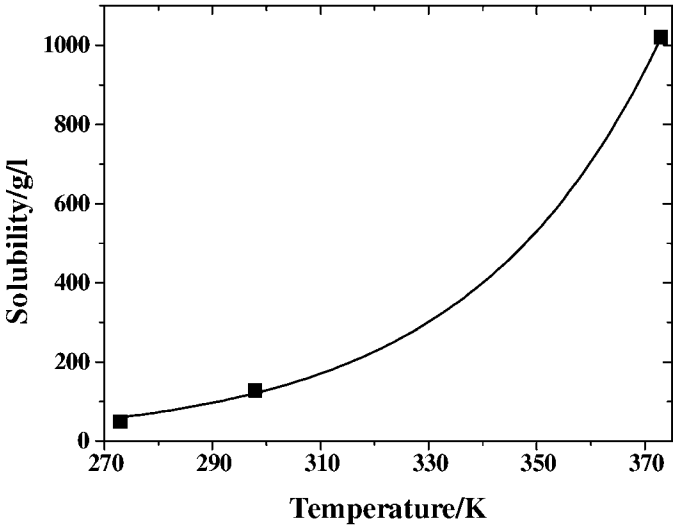

Figure 1
Solubility of $K_2Cr_2O_7$ between 273 and 373 K.

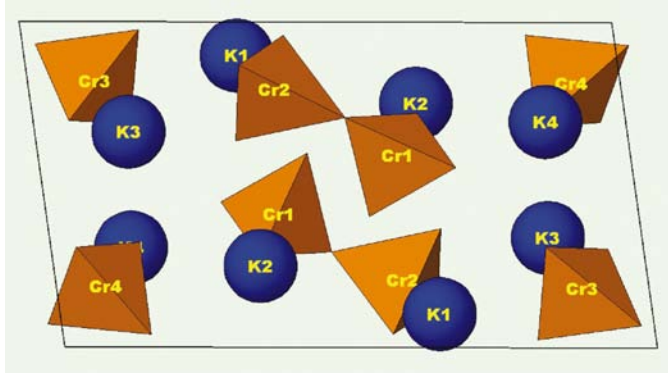

Figure 3
Structure of II-$K_2Cr_2O_7$ viewed along the *b* axis with the *c* axis horizontal.

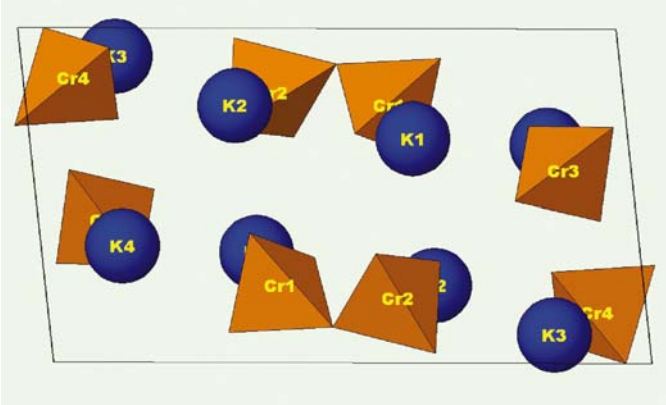

Figure 2
Structure of II-$K_2Cr_2O_7$ viewed along the *a* axis with the *c* axis horizontal.

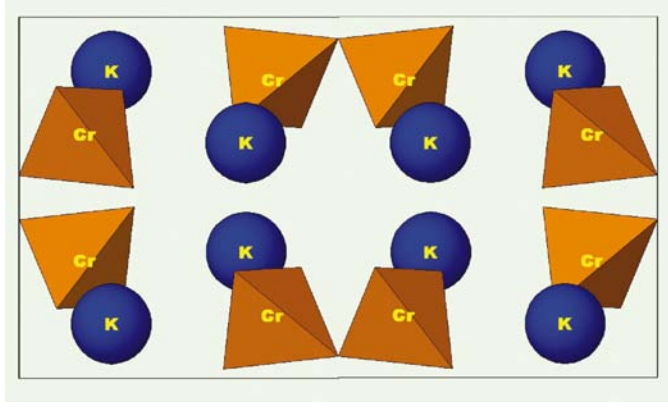

Figure 4
Structure of II*b*-$K_2Cr_2O_7$ viewed along the *a* axis with the $\bar{c}$ axis horizontal.

Table 3
Selected distances (Å) and angles (°) in II-$K_2Cr_2O_7$.

K—O, *n*: *n* is the number of $d_{K-O} \leq 3.5$ Å.

Cr—O	Crystal 1 d_{Cr-O} (Å)	Crystal 2 d_{Cr-O} (Å)	K—O, *n*	Crystal 1 $\langle d_{K-O}\rangle$ (Å)	Crystal 2 $\langle d_{K-O}\rangle$ (Å)
Cr1—O1	1.6144 (17)	1.611 (2)	K1—O, 7	2.692–2.875	2.687–2.879
Cr1—O2	1.6158 (17)	1.613 (3)		2.76 (8)†	2.76 (8)
Cr1—O3	1.6036 (17)	1.604 (3)			
Cr1—O4	1.7884 (16)	1.788 (3)	K2—O, 10	2.743–3.303	2.746–3.308
Cr2—O4	1.7844 (16)	1.782 (2)		2.96 (19)	2.96 (19)
Cr2—O5	1.6181 (16)	1.615 (2)			
Cr2—O6	1.6110 (17)	1.614 (3)	K3—O, 9	2.751–3.065	2.749–3.064
Cr2—O7	1.6035 (17)	1.605 (3)		2.88 (9)	2.88 (9)
Cr3—O8	1.6216 (16)	1.618 (3)			
Cr3—O9	1.6141 (16)	1.615 (2)	K4—O, 8	2.748–3.134	2.752–3.138
Cr3—O10	1.6034 (17)	1.606 (3)		2.89 (13)	2.89 (13)
Cr3—O11	1.7795 (16)	1.778 (2)			
Cr4—O11	1.7877 (15)	1.787 (2)			
Cr4—O12	1.6213 (16)	1.619 (3)	Cr1—O4—Cr2	126.91 (10)	127.29 (14)
Cr4—O13	1.6030 (17)	1.604 (3)			
Cr4—O14	1.6195 (16)	1.619 (2)	Cr3—O11—Cr4	123.97 (8)	124.19 (13)

† Range, mean d_{K-O} and uncertainty as calculated by Bessel's method.

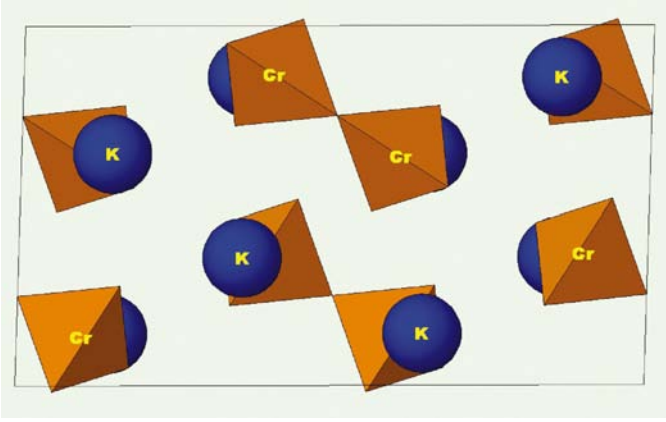

Figure 5
Structure of II*b*-$K_2Cr_2O_7$ viewed along the *b* axis with the $\bar{c}$ axis horizontal.

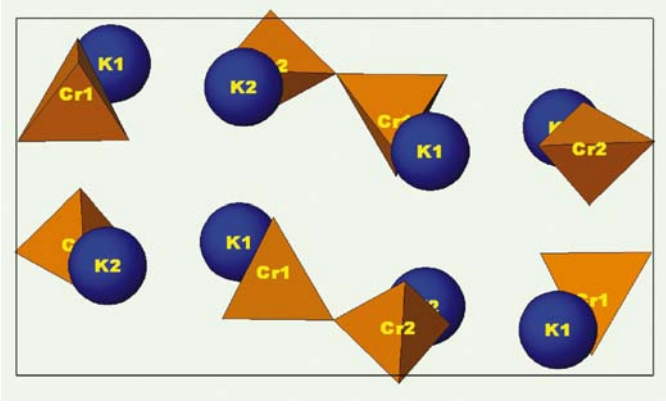

Figure 6
Predicted-phase I-$K_2Cr_2O_7$ structure viewed along the *a* axis with the *c* axis horizontal.

3.4. Bond lengths and valence

The weighted mean over all terminal distances in Table 5 is $\langle d_{Cr-O}\rangle$ = 1.62 (3) Å, including those in isolated ions such as $K_4(CrO_4)(NO_3)_2$ (Kolitsch, 2002) and $C_4H_{12}N_2(CrO_4)$ (Srinivasam *et al.*, 2003), and in the di-, tri- and tetrachromates. The corresponding bridging $\langle d_{Cr-O}\rangle$ is 1.76 (3) Å, excluding the length for $Na_2Cr_2(AsO_4)_3$ in Table 5, in agreement with the values in II-$K_2Cr_2O_7$.

The bond-valence (b.v.) sums (Brown & Altermatt, 1985) for each atom in II-$K_2Cr_2O_7$, based on the determination of crystal 1, are 5.89–5.95 (4) for Cr; 1.09–1.31 (3) for K; 2.16, 2.18 (2) for bridging Cr—O—Cr atoms O(4), O(11) and 1.89–2.05 (2) for the remaining O atoms. The uncertainties in b.v. may be underestimated.[5] The agreement with expectation is satisfactory for Cr, although it may be influenced by the inclusion of earlier $K_2Cr_2O_7$ results in the derivation of the value of r_0 for Cr^{6+} and O^{2-}.

The corresponding b.v. sums in II*b*-$K_2Cr_2O_7$, based on the determination by Krivovichev *et al.* (2000), are 5.88 for Cr, 1.16 for K, 2.06 for the bridging O3 atom and 1.90–2.00 for the remaining O atoms, in good agreement with the results for phase II. The large uncertainties in the predicted bond lengths of phase I preclude the derivation of useful b.v. values.

4. Comparison of present and previous II-$K_2Cr_2O_7$ structure determinations

A plot of the ordered experimental quantiles $Q_{exp} = |\xi_i(1) - \xi_i(2)|/\{\sigma^2[\xi_i(1)] + \sigma^2[\xi_i(2)]\}^{1/2}$, where $\xi_i(1)$ and $\xi_i(2)$ are the *i*th parameters from the first and second independent determinations, and $\sigma(\xi_i(1))$ and $\sigma(\xi_i(2))$ the corresponding standard uncertainties (s.u.s) in each parameter, against the corresponding normal quantiles Q_{norm}, allows quantitative comparison of the results (Abrahams & Keve, 1971). The Q_{norm} magnitudes are conveniently calculated by the program *NORMPA* (Ross, 2003). Crystal structure determinations of II-$K_2Cr_2O_7$ have been reported by Kuz'min *et al.* (1967, 1969), Brandon & Brown (1968) and Brunton (1973). The atomic coordinates of Kuz'min and co-workers are without s.u.s, hence the resulting Q_{exp} cannot be evaluated nor normal probability analysis applied. Atomic coordinates from the other two studies and those in §3 on crystals 1 and 2 are compared in the following six $Q_{exp} - Q_{norm}$ pairwise combinations.

The close approach to linearity of the $Q_{exp} - Q_{norm}$ array in Fig. 8, based on the atomic coordinates determined on crystal 1 (see §3.1) and those of Brandon & Brown (1968), with the slope and intercept as in Table 6, indicates an error distribution close to normal with joint s.u.s (j.s.u.s) underestimated by a factor of *ca* 2.5. Comparable results follow from the $Q_{exp} - Q_{norm}$ array in Fig. S2, based on the atomic coordinates

[5] Assuming 1 s.u. for each bond length and the same displacement sense for all bonded atoms.

Table 4
Predicted atomic coordinates for Phase I.

Phase I: coordinate uncertainties estimated as *ca* 1 Å.

	x	*y*	*z*
Cr1	0.6392	0.7107	0.5952
Cr2	0.7379	0.8663	0.4001
K1	0.1330	0.6272	0.6494
K2	0.2226	0.8074	0.3569
O1	0.7641	0.5559	0.5963
O2	0.6890	0.8420	0.6768
O3	0.4712	0.6229	0.5971
O4	0.6389	0.8447	0.5021
O5	0.8852	0.7338	0.3895
O6	0.8370	1.0230	0.3998
O7	0.5794	0.8567	0.3184

determined with crystal 2 and those of Brandon & Brown (1968) in which the error distribution is again close to normal, with j.s.u.s underestimated by a factor of *ca* 2.3. Comparison of the atomic coordinates determined on crystals 1 and 2 in Fig. 9 also indicates an error distribution close to normal. Figs. 8, 9 and S2 show that the present results are consistent with Brandon & Brown (1968) if the s.u.s in the latter are underestimated by a factor of *ca* 2, and the s.u.s in crystals 1 and 2 overestimated by a factor of *ca* 1.2 (*i.e. ca* 1/0.86).

The corresponding $Q_{\rm exp} - Q_{\rm norm}$ comparison of crystal 1 and Brunton's (1973) atomic coordinates is presented in Fig. S3, that of crystal 2 and Brunton's in Fig. S4, with that of Brandon & Brown's (1968) and Brunton's in Fig. S5. Each distribution in Figs. S2–S5 is close to normal with the indicators in Table 6 showing the j.s.u.s in Figs. S3 and S4 to be underestimated by a factor of *ca* 1.7. The s.u. underestimation factor of *ca* 2.2 in Fig. S5 together with the slight overestimation factor noted between crystals 1 and 2 supports the deduction that the underestimates arise primarily in the earlier work.

The results above demonstrate clearly that all four sets of refined atomic coordinates for II-$K_2Cr_2O_7$ are substantially free from systematic error. The experimental uncertainties should be corrected in each case by factors derived from the magnitudes of the slopes listed in Table 6.

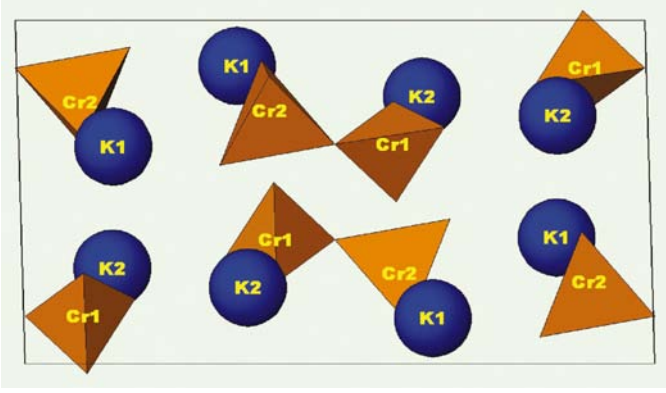

Figure 7
Predicted-phase I-$K_2Cr_2O_7$ structure viewed along the *b* axis with the *c* axis horizontal.

Table 5
Selected recent literature distances (Å) in chromates with terminal and bridging distances except for isolated anions.

Uncertainties in averaged distances by Bessel's method.

Compound	Reference	$\langle d_{\rm Cr-O}\rangle_{\rm term}$	$\langle d_{\rm Cr-O}\rangle_{\rm bridg}$
$K_4(CrO_4)(NO_3)$	Kolitsch (2002)	1.645 (4)	–
$(C_4H_{12}N_2)[CrO_4]$	Srinivasam *et al.* (2003)	1.65 (2)	–
$[(CH_3)_3CNH_3]_2[CrO_4]$	Chebbi & Driss (2002)	1.626 (8)†	–
$CuCrO_4$	Seferiadis & Oswald (1987)	1.599 (3)	1.731 (2)
II*b*-$K_2Cr_2O_7$	Krivovichev *et al.* (2000)	1.616 (10)	1.782 (1)
$[(CH_3)_3SO]_2Cr_2O_7$	Jannin *et al.* (1993)	1.57 (4)	1.777 (14)
$Na_3Cr_2(AsO_4)_3$	Bouzemi *et al.* (2002)	–	1.994 (2)‡
$(CN_3H_6)_2Cr_3O_{10}$	Stępień & Grabowski (1977)	1.65 (2)	1.75 (6)
$Cs_2Cr_4O_{13}$	Kolitsch (2004)	1.588 (13)	1.77 (6)

† Disordered CrO_4^{2-} anion over two sets of sites, with a Cr—Cr separation of 0.9 Å. ‡ Cubic crystal with fully connected extended structure.

5. Phase transitions in $K_2Cr_2O_7$

In reporting the structure of monoclinic $K_2Cr_2O_7$ (II*b*), Krivovichev *et al.* (2000) suggested it may be related to that of phase II by the rotation of alternate layers to give the observed *A*2/*a* symmetry; they also gave the unit-cell volume V(II*b*-$K_2Cr_2O_7)_{293\,K}$ as 717.38 (17) Å^3. Crystal I has V(II-$K_2Cr_2O_7)_{296\,K}$ = 725.37 (16) Å^3, hence $\Delta V_{\rm II\text{-}IIb}$ = 0.011, significantly less than the difference reported previously, see §1.

5.1. Phase nomenclature

The ambiguity arising from earlier designations of the high-temperature monoclinic (I) in addition to the ambient

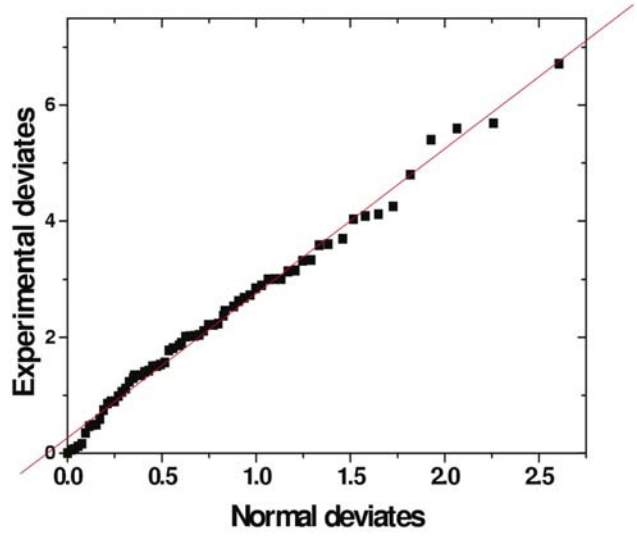

Figure 8
Normal probability, $Q_{\rm exp} - Q_{\rm norm}$, plot for the atomic coordinates determined with crystal 1 of II-$K_2Cr_2O_7$ *versus* those reported by Brandon & Brown (1968).

Table 6
Linear-regression indicators for the II-$K_2Cr_2O_7$ $Q_{exp} - Q_{norm}$ plots.

$\xi(1)$	$\xi(2)$	Slope	Intercept	Correlation coefficient
Crystal 1	Brandon & Brown (1968)	2.49 (3)	0.27 (3)	0.995
Crystal 1	Crystal 2	0.86 (1)	0.0001 (14)	0.991
Crystal 2	Brandon & Brown (1968)	2.30 (2)	0.12 (2)	0.997
Crystal 1	Brunton (1973)	1.65 (3)	−0.10 (3)	0.989
Crystal 2	Brunton (1973)	1.72 (5)	−0.28 (5)	0.977
Brandon & Brown (1968)	Brunton (1973)	2.19 (3)	0.07 (3)	0.994

temperature monoclinic (II*b*) and triclinic (II) structures as the β-phase is lifted by following IUCr's nomenclature (see *Appendix A*). The designation '*b*' rather than 'III' indicates the formation of phase II*b* in a different branch than that of phase II, see §1. The phase at $T_{PT} \geq 544$ K for crystals grown from aqueous solution is thus denoted as I-$K_2Cr_2O_7$, that at $T_{PT} \leq 502$ K as II-$K_2Cr_2O_7$. The transition temperature from phase II to phase I for the anhydrous material is T_{PT} = 531 (2) K, see §5.3.

5.2. Thermogravimetry

Measurement with a Perkin–Elmer Pyris-1 TGA reveals that $K_2Cr_2O_7$ crystals (with mass typically around 15 mg), grown from aqueous solution undergo no loss that exceeds the instrumental sensitivity (±2 µg) on first heating to $T \simeq 531$ K. A sharp and reproducible mass loss of *ca* 0.05% then commenses, continuing until *ca* 545 K and proceeding thereafter at a rate reduced by a factor of *ca* 2 until *ca* 660 K for a total loss of *ca* 0.20%, see Fig. 10(*a*). Cooling the same sample to 300 K and then reheating results in no further mass loss. The rapid mass loss becomes more gradual as the crystalline particle size is reduced by grinding. Reproducible mass changes of $\lesssim 0.1\%$ on heating or cooling over the entire thermal range are due to buoyancy effects.

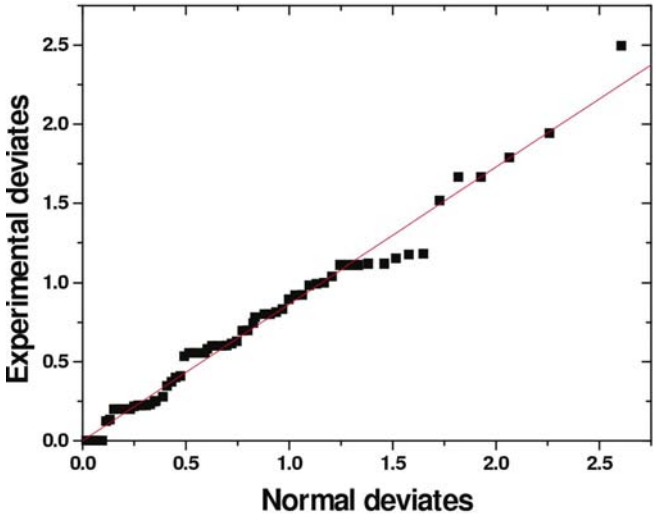

Figure 9
Normal probability $Q_{exp} - Q_{norm}$ plot for the atomic coordinates determined with crystal 1 *versus* crystal 2 of II-$K_2Cr_2O_7$.

5.3. Differential scanning calorimetry

The thermal hysteresis and entropy change at T_{PT} measured with a Perkin–Elmer DSC-7 at rates ranging from 1 to 100 K min^{-1} are in basic agreement with earlier reported values, see §1.[6] All transition temperatures that follow are at endotherm onset, with corresponding peak values 6.1 (2) K higher; each one has been corrected for instrumental hysteresis by extrapolation to a heating rate of 0 K min^{-1} and is reproducible over numerous samples. The phase transition temperature observed on first heating solution-grown samples is 544 (2) K. The exothermic transition on cooling is consistently observed thereafter at 502 (2) K. The endothermic transition on second and all subsequent heatings is 531 (2) K, see Fig. 10(*b*). The break in Fig. 10(*b*) between exotherm and endotherm sections is in recognition of the differences in absolute entropic background, displayed in the figure as 0 J mol^{-1} K^{-1}. The thermal hysteresis ranges from *ca* 32 K at the lowest to *ca* 80 K at the highest heating rate, extrapolating to *ca* 29 K under isothermal conditions; thermal hysteresis is indicative of a first-order phase transition.

The entropy change both at initial and subsequent T_{PT} is $\langle \Delta S \rangle$ = 4.0 (1) J mol^{-1} K^{-1}. All exotherms are *ca* 50% wider than endotherms, see §6.2 for an explanation. The possibility that relaxation might influence T_{PT} was investigated by remeasuring a sample equilibrated in the DSC at 373 K for 1 h, then a further 10 h both with and without N_2 purge following the completion of a normal measurement cycle. The initial and subsequent endotherms remained identical at 531 (2) K, consistent with the elimination of all included water.

5.4. Optical microscope observations at T_{PT}

Brown (2003) noted that crystals of phase II placed 'on a microscope slide jump on being heated through the phase transition as the color changes from orange–red to deep red, almost black'. Small single crystals of phase II viewed under polarized light transmission in a Jenalab POL microscope, using an MK1 (Instec, Inc.) heating stage, exhibited a color change from strongly reddish-orange to very deep red (see footnote **2**) at *ca* 549 K. Further heating to *ca* 553 K causes the crystal to fracture and simultaneously move. Crystal movement was again notable between 499 and 492 K on cooling, the material remaining very deep red. The crystals are observed to melt at 683 (2) K on heating and recrystallize at 636 (2) K on cooling under a heating/cooling rate of 50 K min^{-1} for an isothermal T_{melt} = 660 (2) K. Further color change was not observed. The experimental uncertainty in temperature due to thermal gradients is *ca* 5 K. Decomposition begins at *ca* 775 K (Weast *et al.*, 1988).

[6] Following an exploratory scan from 300 to 600 to 300 K, in which the endotherm at 544 K and exotherm at 502 K were the only thermal events, all subsequent calorimetric scans were from 375 to 575 to 375 K, then repeated two additional times as a reproducibility check.

6. Atomic displacement analysis of the $K_2Cr_2O_7$ phase transitions

Conversion of the experimental or inferred atomic *xyz* coordinates of phases II, II*b* or I to Cartesian *XYZ* coordinates, with $X||a$ and $Z||c^*$ in Å, allows the evaluation of the component and the total coordinate differences between phases. Such a transformation is readily made by means of *CALCRYS* (Urzhumtseva & Urzhumtsev, 2000). All individual atomic changes in location between phases are given in Table 7. A comparison of Cartesian atomic coordinates is made without origin shift, since the origin in all phases is defined by an inversion center.

6.1. Is a transition possible from phase II*b* to phase II?

The transition at *ca* 325 K from phase II*b* suggested by Kozlova *et al.* (1978) is presently without experimental confirmation, although such a transition is allowed either to phase I or phase II by the supergroup 2/*m*, subgroup $\overline{1}$, relationship. In addition, the unit-cell parameters in all three phases are comparable, as are the coordinates of corresponding atoms following unit-cell transposition as in Table 1. The experimental atomic coordinates of phases II*b* and II are presented in Table S1, with the four O atoms in each tetrahedron shown in brackets; O3 in phase II*b* and O4 and O11 in phase II are shared by pairs of tetrahedra to form $Cr_2O_7^{2-}$ ions. Cartesian coordinates of both phases are given in Table S2.

The maximum atomic displacement magnitude reported in reversible solid-state phase transitions is *ca* 1.5 Å (Abrahams, 2003). Both component and total atomic coordinate displacements for many of the independent atoms between phases II*b* and II exceed this limit with high significance, see Table 7. These positional differences are equivalent to angular changes such as those between the normal to the Cr—O—Cr plane in each phase; for the $Cr1O_4$ and $Cr2O_4$ tetrahedra that change is 13°, whereas for the $Cr3O_4$ and $Cr4O_4$ tetrahedra it is 75°. Each of the $Cr1O_4$ and $Cr2O_4$ tetrahedra rotate 16 and 11°, the $Cr3O_4$ and $Cr42O_4$ tetrahedra rotate 67 and 81° around their respective $Cr—O_{shared}—$ axes, see Figs. 3 and 5. The orientation change in the Cr···Cr vector of both $Cr_2O_7^{2-}$ ions is 14°. Both phase determinations were at ambient temperatures, close to the proposed transition at *ca* 325 K, hence any changes in atomic coordinates are expected to be relatively small at this transition. Atomic position changes of the magnitudes noted are highly unlikely as, therefore, is the possibility of such a transition.

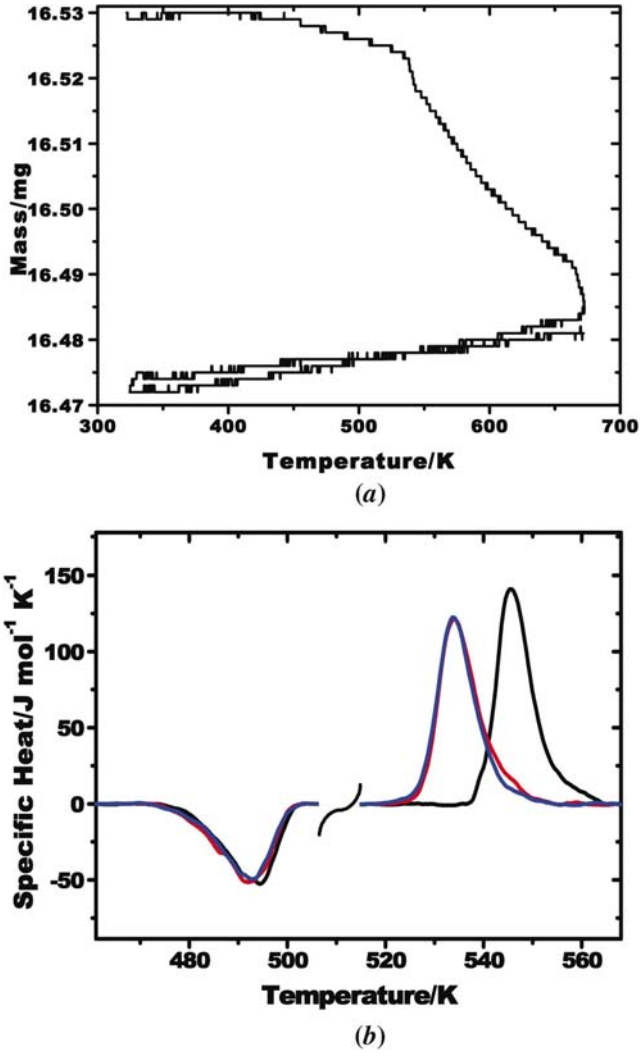

Figure 10
(*a*) Thermogravimetric variation between 325 and 673 K, then cooling and reheating. (*b*) Endotherms on first (red) and second (black) heating.

6.2. The transition from phase II to phase I

The rotation, at this phase transition, of *ca* 60° by the three terminal O atoms in each tetrahedron about the $O_{shared}—Cr—$ axis, with respect to the Cr—O—Cr plane, has three major components. The two sets of three terminal O atoms in the $Cr1Cr2O_7^{2-}$ ion undergo direct rotations of 28 and 24°, as derived from the Cartesian coordinates in Table S3, those in the $Cr3Cr4O_7^{2-}$ ion rotations of 24 and 25°. The Cr1···Cr2 vector orientation changes by 21° and the Cr3···Cr4 vector by 49° at the transition; the dihedral angle between Cr1—O—Cr2 in phases I and II, and that between Cr3—O—Cr4 in the two phases each change 46° at the transition. In consequence, the $Cr_2O_7^{2-}$ ion undergoes a conformation change.

The $O—Cr—O_{shared}—Cr—O$ sequence in II-$K_2Cr_2O_7$ and $(NH_4)_2Cr_2O_7$ reported by Brown & Calvo (1970) approximates *mm* symmetry with the three O atoms in the sequence nearly linear, as is also the case in phase II*b*. By contrast, one of the two independent $Cr_2O_7^{2-}$ ions in $SrCr_2O_7$ (Wilhelmi, 1967) has this configuration but the second, independent, $Cr_2O_7^{2-}$ ion has an $O—Cr—O_{shared}—Cr—O$ sequence close to *mm* symmetry, but with the $—CrO_3$ groups rotated by *ca* 60°. The conformation of the $Cr_2O_7^{2-}$ ion in phase I, with a twist angle of *ca* 7.6° from *mm* symmetry, is very close to that of the second ion in $SrCr_2O_7$. The existence of two ions in $SrCr_2O_7$, each approximating *mm* symmetry but with different conformations, suggests both arrangements occupy similar energy states. The conformation of the $Si_2O_7^{6-}$ ion in the mineral hemimorphite, $Zn_4Si_2O_7(OH)_2·H_2O$ (Cooper *et al.*, 1981), is

Table 7
Component $|\Delta(\xi)|$ and total $|(\Delta(XYZ)|$ differences between identical atoms in phases I, II and II*b* of $K_2Cr_2O_7$, in Å.

See also Table 1 and Tables S2–S4.

	Phases I and II				Phases II and II*b*				Phases II*b* and I			
	$\Delta(X)$	$\Delta(Y)$	$\Delta(Z)$	$\Delta(XYZ)$	$\Delta(X)$	$\Delta(Y)$	$\Delta(Z)$	$\Delta(XYZ)$	$\Delta(X)$	$\Delta(Y)$	$\Delta(Z)$	$\Delta(XYZ)$
Cr1	1.46	0.51	0.16	1.55	1.87	1.24	0.15	2.26	0.41	0.75	0.01	0.85
Cr2	0.44	1.11	0.18	1.21	1.66	0.68	0.28	1.81	1.22	−0.42	−0.10	1.30
Cr3	0.05	0.25	0.18	0.32	0.98	0.61	0.16	1.16	–	–	–	–
Cr4	0.40	0.32	0.16	0.54	0.27	1.14	0.24	1.20	–	–	–	–
K1	1.44	0.67	0.12	1.59	1.97	0.75	0.04	2.11	0.53	0.08	−0.16	0.56
K2	0.44	0.87	0.10	0.98	1.72	0.41	0.02	1.76	1.27	−1.27	−0.07	1.80
K3	0.12	0.09	0.12	0.19	0.27	0.24	0.20	0.42	–	–	–	–
K4	0.21	0.14	0.10	0.27	1.02	1.20	0.10	1.58	–	–	–	–
O1	1.51	0.57	0.70	1.76	2.08	1.57	0.07	2.61	0.57	1.00	0.77	1.39
O2	1.47	0.58	0.33	1.61	1.73	1.44	0.39	2.28	−0.54	0.86	−0.06	1.01
O3	1.46	0.38	0.68	1.65	1.98	0.81	0.09	2.14	0.52	0.43	−0.59	0.90
O4	0.50	0.47	0.33	0.76	1.69	1.05	0.43	2.04	1.19	0.58	−0.10	1.33
O5	0.36	1.14	0.71	1.39	1.62	0.73	0.09	1.78	1.26	−0.41	0.62	1.46
O6	0.54	0.98	0.52	1.24	1.62	0.48	0.58	1.79	1.08	−0.51	−1.10	1.62
O7	0.28	1.75	0.24	1.79	1.57	0.49	0.04	1.65	1.30	−1.26	0.20	1.81
O8	0.15	0.18	0.70	0.74	1.11	0.52	1.40	1.86	–	–	–	–
O9	0.12	0.89	0.24	0.93	1.15	0.31	0.29	1.23	–	–	–	–
O10	0.02	0.27	0.52	0.58	0.94	2.70	1.31	3.15	–	–	–	–
O11	0.28	0.42	0.33	0.60	1.18	1.08	0.30	1.63	–	–	–	–
O12	0.53	0.42	0.70	0.97	1.23	1.57	0.19	2.00	–	–	–	–
O13	0.45	0.25	0.68	0.85	0.34	0.49	2.21	2.29	–	–	–	–
O14	0.95	0.31	0.33	1.05	0.07	0.77	0.12	0.78	–	–	–	–

similar to that in phase I and is indicative of it having high stability.

Brown & Calvo (1970) proposed that alternate layers in II-$K_2Cr_2O_7$ undergo a pseudorotation of *ca* 90° about c^* in the transition from phase I to phase II such that 'a perpendicular vector from the Cr···Cr line through the bridging O atom moves from the *a* to the *b* direction' (Brown, 2004). The atomic displacements greater than 2 Å required by their model, the clear evidence of a higher residual symmetry present in phase II, and the confirmation of the characteristic phase I conformation for $Cr_2O_7^{2-}$ provided by $SrCr_2O_7$ and $Zn_4Si_2O_7(OH)_2{\cdot}H_2O$ lend strong support to the stability of the present model.

No difference between corresponding atomic positions in phases I and II exceeds the limit $\Delta(xyz)_{\max} \lesssim 1.5$ Å by more than 3 estimated uncertainties, see Table 7; Cartesian coordinates for all atoms in these two phases are given in Table S3. The relative rotation of *ca* 60° by CrO_4 groups and the effective $\Delta(xyz)$ limit are fully consistent with the first-order phase transition apparent in Fig. 10(*b*). The broadened exotherms relative to the endotherms noted in §5.3 may be due to differences in the kinetics of tetrahedral rotation and ionic displacement required in the transition from phase II to I *versus* those from phase I to II.

The mass loss at T_{PT} of *ca* 0.20% on first heating phase II, see §5.2 and Fig. 10(*a*), is attributed to water since as-grown crystals dehydrated by heating lose no further mass on reheating, even over long periods in a low humidity environment. No difference is observed either in the mass lost or in T_{PT} between first and second heatings of untreated as-grown crystals and those exposed overnight to high humidity. The maximum mass loss due to water corresponds to 1 mol H_2O per *ca* 31 mol $K_2Cr_2O_7$, a ratio that eliminates the possibility of water of hydration.[7] It is hence assumed that growth from aqueous solution results in water-occupied inclusion defects.

The combination of superheated included-water and multiple crack formation likely caused by abrupt changes in unit-cell dimensions associated with the first-order phase transition critically affects T_{PT} in the initial thermal cycle. The Clausius–Clapeyron equation gives the water pressure within an intact inclusion at 531 K as *ca* 5 Mpa. Phase-transition temperatures generally increase with applied pressure. In strongly ionic inorganic oxides such as $La_{1.2}Ca_{1.8}Mn_2O_7$, linear increases of *ca* 1 K every 100 GPa are reported (Kanenev *et al.*, 1997), with smaller increases in more readily deformable materials such as dialkyl-biphenyl compounds of *ca* 1 K MPa^{-1} (Urban *et al.*, 2002). If the application of *ca* 5 MPa raises the barrier to the tetrahedral rotations and ionic displacements required at T_{PT} by *ca* 13 K, then the phase transition would occur at 544 K with the resulting crack initiation, the release of superheated steam and a visible crystal motion, see §5.4. Experimental investigation of the T_{PT}–pressure dependence in $K_2Cr_2O_7$ is appropriate.

6.3. Structural transition from phase II*b* to predicted phase I

Table 7 shows that no atomic position in phase II*b* differs from that inferred for the same atom in phase I by more than the limit $\Delta(xyz)_{\max} \lesssim 1.5$ Å; the K2 and O7 differences are

[7] The only known alkali chromate or dichromate hydrates are $Na_2CrO_4{\cdot}10H_2O$ and $Na_2Cr_2O_7{\cdot}2H_2O$. The difference between the IR spectrum of as-grown and dehydrated phase II crystals, recorded with a Perkin Elmer Spectrum One FT-IR spectrometer and Universal ATR Sampling Accessory with ZnSe crystal, was found to be less than that attributable to instrumental sensitivity.

without significance. Cartesian coordinates for all atoms in phases I and II*b* are given in Table S4. The rotations of the $-CrO_3$ group about the $O_{shared}-Cr-$ bond by 31 and 34°, the 25° change in Cr···Cr vector direction and the 34° difference between normals to the Cr—O—Cr plane at a transition between phases II*b* and I are comparable to those in the transition from phases II to I. A transition that is probably of first order is hence to be expected. If, however, $T_{PT} \ll 531$ K, as suggested by Kozlova *et al.* (1978), then a new phase is expected to intervene between phases II*b* and I since a lower value for T_{PT} would require phase I to be stable well below its thermal limit.

6.4. Additional $K_2Cr_2O_7$ phase formation

Effective rotations as large as 60° about the $CrO_{shared}-$ bond by $-CrO_3$ and atomic displacements as large as *ca* 1.5 Å in the transition between phases I and II, and also between phases I and II*b*, open the possibility of additional phase formation as the potential surface that mediates crystal growth is perturbed by the presence of other ions, leading to an equilibrium change. Recent reports of the growth of large (4.5 mm diameter, 60 mm length), mostly right-handed, helical $K_2Cr_2O_7$ polycrystals from aqueous gels (Suda & Matsushita, 2004; Suda *et al.*, 2000) may be examples of additional phases. Glutamic or aspartic acid dissolved in gelatin provides a chiral environment in which left-handed helical $K_2Cr_2O_7$ crystals grow. If the chiral morphology is due to a symmetry change, then the only subgroup enantiomorphic to phase I is 1. Alternatively, the major differences in the appearance and growth rates of (001) and (00$\bar{1}$) noted by Shubnikov (1912, 1931), acting on the component polycrystals, may also result in helical growth. Structural studies on these helical crystals have not yet been reported.

Measurement of the atomic coordinate and lattice parameter thermal dependence of all $K_2Cr_2O_7$ phases over the widest temperature range available will further clarify the phase relationships in $K_2Cr_2O_7$.

APPENDIX *A*

Among the earlier designations for the phases of $K_2Cr_2O_7$ are *A* for phase II, *C* for phase I and *B* for phase II*b* (Jaffray & Labary, 1956), monoclinic high temperature for phase I, triclinic low temperature for phase II and monoclinic metastable for phase II*b* (Klement & Schwab, 1960), β for phase II*b* (Kozlova *et al.*, 1978; Krivovichev *et al.*, 2000), α for phase I and β for phase II (Hess & Eysel, 1989). The IUCr phase transition nomenclature (Tolédano *et al.*, 1998, 2001) was designed both to clarify and amplify such designations. Its application to phases I, II and II*b* of $K_2Cr_2O_7$ results in:

I|660–531 K|$P2_1/n$ (14)|$Z = 4$|non-ferroic|decomposes above *ca* 775 K.

II|531– $\lesssim$ 270 K|$P\bar{1}$ (2)|$Z = 4$|non-ferroic|lower temperature limits not reported.

II*b*|$\gtrsim$325 to $\lesssim$288 K| $A2/a$ (15)|$Z = 4$|non-ferroic|upper and lower temperature limits not reported.

The phase label is given in field 1, the thermal and/or pressure stability limits for the phase in field 2, the space group with the ITA number in field 3, the ferroic property in field 4 and other pertinent data in field 5. In the event a new phase is found to exist between II*b* and I, see §6.3, it would become phase II*b* and the present phase II*b* would become phase III*b*. See §§1 and 5.1 for use of the letter '*b*'.

The contributions of J. E. Stephens, R. D. Wiegel, E. R. Ylvisaker and R. J. Yager were made as Southern Oregon University undergraduates in their senior year. Those of M. Mengis were as a North Medford High School Junior Saturday Academy Apprenticeship in Science & Engineering awardee. It is a pleasure to thank Professor D. C. Johnson and Daniel Ruebusch, University of Oregon, for their kindness in taking X-ray powder diffraction scans, Professor I. D. Brown for communicating his microscope observations on the phase transition and his valuable comments on an earlier draft, Professor H. Wondratschek for the 1830 Mitcherlich paper and his comments, Professor S. V. Krivovichev and Dr E. V. Kir'yanova for discussions of the metastable-phase II*b* preparation, Professor J. Kobayashi for valuable comments on phase relationships and bringing the papers on helical crystals to our attention, Professor A. G. Urzhumtsev and Dr. L. M. Urzhumtseva for their new version of *CALCRYS*, and the National Science Foundation (DMR-9708246, DMR-0137323) for financial support.

References

Abrahams, S. C. (2003). *Acta Cryst.* B**59**, 541–556.
Abrahams, S. C. & Keve, E. T. (1971). *Acta Cryst.* A**27**, 157–165.
Altomare, A., Cascarano, G., Giacovazzo, C., Guagliardi, A., Burla, M. C., Polidori, G. & Camalli, M. (1994). *J. Appl. Cryst.* **27**, 435.
Averbuch-Pouchot, M. T., Durif, A. & Guitel, J. C. (1978). *Acta Cryst.* B**34**, 3725–3727.
Bouzemi, B., Boughzala, H. & Jouini, T. (2002). *Acta Cryst.* E**58**, i117–i118.
Brandon, J. K. & Brown, I. D. (1968). *Can. J. Chem.* **46**, 933–941.
Brown, I. D. (2003). Private communication.
Brown, I. D. (2004). Private communication.
Brown, I. D. & Altermatt, D. (1985). *Acta Cryst.* B**41**, 244–247.
Brown, I. D. & Calvo, C. (1970). *J. Solid State Chem.* **1**, 173–179.
Brunton, G. (1973). *Mater. Res. Bull.* **8**, 271–274.
Carter, R. L. & Bricker, C. E. (1969). *Spectrosc. Lett.* **2**, 247–253.
Chebbi, H. & Driss, A. (2002). *Acta Cryst.* E**58**, m494–m496.
Cooper, B. J., Gibbs, G. V. & Ross, F. K. (1981). *Z. Kristallogr.* **156**, 305–321.
Dowty, E. (2003). *Atoms*, Version 6.1. Shape Software, Kingsport, TN 37663. http://www.shapesoftware.com.
Enraf–Nonius (1993). *CAD-4/PC*, Version 1.2. Enraf–Nonius, Delft, The Netherlands.
Groth, P. (1908). *Chemische Krystallographie*, Vol. II, pp. 584–588. Engelmann: Leipzig.
Hess, S. & Eysel, W. (1989). *J. Thermal Anal.* **35**, 627–635.
Jaffray, J. & Labary, A. (1956). *C. R. Acad. Sci.* **242**, 1421–1422.
Jannin, M., Puget, R., de Brauer, C. & Perret, R. (1993). *Acta Cryst.* C**49**, 749–751.
Kanenev, K. V., Lees, M. R., Balakrishnan, G. & Paul, D. M. (1997). *Phys. Rev. B*, **56**, R12688–R12690.
Kir'yanova, E. V. (2004). Private communication.
Klement, U. & Schwab, G.-M. (1960). *Z. Kristallogr.* **114**, 170–199.
Kolitsch, U. (2002). *Acta Cryst.* E**58**, i88–i90.

Kolitsch, U. (2004). *Acta Cryst.* C**60**, i17–i19.
Kozlova, O. G., Geraskina, G. P. & Belov, N. V. (1978). *Dokl. Akad. Nauk. SSSR*, **240**, 588–590.
Krivovichev, S. V. & Burns, P. (2003). *Z. Kristallogr.* **218**, 725–732.
Krivovichev, S. V., Kir'yanova, E. V., Filatov, S. K. & Burns, P. C. (2000). *Acta Cryst.* C**56**, 629–630.
Kuz'min, E. A., Ilyukhin, V. V., Kharitonov, Yu. A. & Belov, N. V. (1969). *Krist. Technol.* **4**, 441–461.
Kuz'min, E. A., Plyukhin, V. V. & Belov, N. V. (1967). *Dokl. Akad. Nauk SSSR*, **173**, 1068–1071.
Mathur, M. S., Frenzel, C. A. & Bradley, E. B. (1968). *J. Mol. Struct.* **2**, 429–435.
Mitscherlich, E. (1830). *Ann. Phys.* **94**, 168–173.
Molecular Structure Corporation (1997). *TeXsan*, Version 1.8. MSC, 3200 Research Forest Drive, The Woodlands, TX 77381, USA.
Ross, C. R. (2003). *NORMPA*. Unpublished. Department of Structural Biology, St Jude Children's Research Hospital, Memphis, TN 38105–2794, USA.
Schwarzenbach, D., Abrahams, S. C., Flack, H. D., Gonschorek, W., Hahn, Th., Huml, K., Marsh, R. E., Prince, E., Robertson, B. E. Rollett, J. S. & Wilson, A. J. C. (1989). *Acta Cryst.* A**45**, 63–75.
Seferiadis, N. & Oswald, H. R. (1987). *Acta Cryst.* C**43**, 10–12.
Shubnikov, A. V. (1912). *Z. Kristallogr.* **50**, 19–23.
Shubnikov, A. V. (1931). *Z. Kristallogr.* **76**, 469–472.
Silber, C., Breidenstein, B., Heide, G. & Follner, H. (1999). *Cryst. Res. Technol.* **34**, 969–974.
Srinivasan, B. R., Näther, Chr. & Bensch, W. (2003). *Acta Cryst.* E**59**, m639–m641.
Stedehouder, P. L. & Terpstra, P. (1930). *Physica*, **10**, 113–124.
Stępień, A. & Grabowski, M. J. (1977). *Acta Cryst.* B**33**, 2924–2927.
Suda, J. & Matsushita, M. (2004). *J. Phys. Soc. Jpn*, **73**, 300–302.
Suda, J., Matsushita, M. & Izumi, K. (2000). *J. Phys. Soc. Jpn*, **69**, 124–129.
Tolédano, J.-C., Berry, R. S., Brown, P. J., Glazer, A. M., Metselaar, R., Pandey, D., Perez-Mato, J. M., Roth, R. S. & Abrahams, S. C. (2001). *Acta Cryst.* A**57**, 614–626.
Tolédano, J.-C., Glazer, A. M., Hahn, Th., Parthé, E., Roth, R. S., Berry, R. S., Metselaar, R. & Abrahams, S. C. (1998). *Acta Cryst.* A**54**, 1028–1033.
Urban, S., Massalska, M., Würflinger, A. & Czupryński, K. (2002). *Z. Naturforsch. Teil A*, **57**, 641–644.
Urzhumtseva, L. M. & Urzhumtsev, A. G. (2000). *J. Appl. Cryst.* **33**, 992.
Walker, N. & Stuart. D. (1983). *Acta Cryst.* A**39**, 158–166.
Weast, R. R., Astle, M. J. & Beyer, W. H. (1988). *CRC Handbook of Chemistry and Physics.* Boca Raton: CRC Press.
Wilhelmi, K.-A. (1967). *Arkiv Kemi*, **26**, 149–156.
Zachariasen, W. H. (1967). *Acta Cryst.* **23**, 558–564.
Zhukova, L. A. & Pinsker, Z. G. (1964). *Kristallografiya*, **9**, 44–49.